^{15}O PET Measurement of Blood Flow and Oxygen Consumption in Cold-Activated Human Brown Fat

Otto Muzik[1,2], **Thomas J. Mangner**[1], **William R. Leonard**[3], **Ajay Kumar**[1], **James Janisse**[4], and **James G. Granneman**[5]

[1]Department of Pediatrics, Wayne State University, Detroit, Michigan

[2]Department of Radiology, Wayne State University, Detroit, Michigan

[3]Department of Anthropology, Northwestern University, Evanston, Illinois

[4]Pathology and Family Medicine, Wayne State University, Detroit, Michigan

[5]Department of Psychiatry and Behavioral Neurosciences, Wayne State University, Detroit, Michigan

Abstract

Although it has been believed that brown adipose tissue (BAT) depots disappear shortly after the perinatal period in humans, PET imaging using the glucose analog ^{18}F-FDG has shown unequivocally the existence of functional BAT in adult humans, suggesting that many humans retain some functional BAT past infancy. The objective of this study was to determine to what extent BAT thermogenesis is activated in adults during cold stress and to establish the relationship between BAT oxidative metabolism and ^{18}F-FDG tracer uptake.

Methods—Twenty-five healthy adults (15 women and 10 men; mean age ± SD, 30 ± 7 y) underwent triple-oxygen scans (H_2^{15}O, C^{15}O, and ^{15}O$_2$) as well as measurements of daily energy expenditure (DEE; kcal/d) both at rest and after exposure to mild cold (15.5°C [60°F]) using indirect calorimetry. The subjects were divided into 2 groups (high BAT and low BAT) based on the presence or absence of ^{18}F-FDG tracer uptake (standardized uptake value [SUV] > 2) in cervical–supraclavicular BAT. Blood flow and oxygen extraction fraction (OEF) were calculated from dynamic PET scans at the location of BAT, muscle, and white adipose tissue. Regional blood oxygen saturation was determined by near-infrared spectroscopy. The total energy expenditure during rest and mild cold stress was measured by indirect calorimetry. Tissue-level metabolic rate of oxygen (MRO$_2$) in BAT was determined and used to calculate the contribution of activated BAT to DEE.

Results—The mass of activated BAT was 59.1 ± 17.5 g (range, 32–85 g) in the high-BAT group (8 women and 1 man; mean age, 29.6 ± 5.5 y) and 2.2 ± 3.6 g (range, 0–9.3 g) in the low-BAT group (9 men and 7 women; mean age, 31.4 ± 10 y). Corresponding maximal SUVs were significantly higher in the high-BAT group than in the low-BAT group (10.7 ± 3.9 vs. 2.1 ± 0.7, P = 0.01). Blood flow values were significantly higher in the high-BAT group than in the low-BAT group for BAT (12.9 ± 4.1 vs. 5.9 ± 2.2 mL/100 g/min, P = 0.03) and white adipose tissue (7.2 ±

3.4 vs. 5.7 ± 2.3 mL/100 g/min, $P = 0.03$) but were similar for muscle (4.4 ± 1.9 vs. 3.9 ± 1.7 mL/100 g/min). Moreover, OEF in BAT was similar in the 2 groups (0.51 ± 0.17 in high-BAT group vs. 0.47 ± 0.18 in low-BAT group, $P = 0.39$). During mild cold stress, calculated MRO_2 values in BAT increased from 0.97 ± 0.53 to 1.42 ± 0.68 mL/100 g/min ($P = 0.04$) in the high-BAT group and were significantly higher than those determined in the low-BAT group (0.40 ± 0.28 vs. 0.51 ± 0.23, $P = 0.67$). The increase in DEE associated with BAT oxidative metabolism was highly variable in the high-BAT group, with an average of 3.2 ± 2.4 kcal/d (range, 1.9–4.6 kcal/d) at rest, and increased to 6.3 ± 3.5 kcal/d (range, 4.0–9.9 kcal/d) during exposure to mild cold. Although BAT accounted for only a small fraction of the cold-induced increase in DEE, such increases were not observed in subjects lacking BAT.

Conclusion—Mild cold-induced thermogenesis in BAT accounts for 15–25 kcal/d in subjects with relatively large BAT depots. Thus, although the presence of active BAT is correlated with cold-induced energy expenditure, direct measurement of MRO_2 indicates that BAT is a minor source of thermogenesis in humans.

Keywords

Brown adipose tissue (BAT, or brown fat) is a thermogenic organ that plays a critical role in nonshivering thermogenesis (1,2). Most mammals, including humans, have abundant BAT during the perinatal period (3,4); however, prominent depots disappear shortly after the perinatal period in several species, and it has been widely assumed the same was true for humans. Recently, numerous papers have appeared in the PET literature identifying symmetric foci of intense uptake of ^{18}F-FDG in humans, and correlative CT clearly indicates that these sites are adipose tissue. Indeed, a recent series of papers has unequivocally demonstrated the existence of functional BAT in humans, suggesting that most, if not all, humans have some functional BAT (5–7).

It is clear that β-adrenergic agonists increase fat oxidation and thermogenesis in humans and that activation of BAT in humans (as assessed by ^{18}F-FDG uptake) is sensitive to adrenergic activation. However, it is not known whether, and to what extent, the increase in ^{18}F-FDG uptake in fact represents an increase in thermogenesis. Therefore, it is critical to directly establish the relationship between BAT oxidative metabolism and ^{18}F-FDG uptake, which is a widely used but indirect and ambiguous measure (8,9). In addition, it is important to determine the quantitative contribution of BAT thermogenesis to total energy expenditure both in the resting state and during physiologic activation by mild cold stress to judge the potential of BAT thermogenesis in contributing to weight loss in obese patients. Thus, the objective of this study was to determine, using dynamic ^{15}O PET imaging, to what extent BAT thermogenesis can be activated in adults during mild cold stress and to establish the relationship between BAT oxidative metabolism and ^{18}F-FDG uptake.

MATERIALS AND METHODS

Subjects

The report expands preliminary observations of similar design made in 14 subjects (10) and extends this analysis to include near-infrared spectroscopy (NIRS). A total of 25 healthy adults (15 women and 10 men; mean age $\pm$ SD, 30 ± 7 y) were studied. Stature was measured to the nearest centimeter and weight to the nearest 0.5 kg, following the standard procedures of Lohman et al. (11). The body mass index was calculated as weight divided by height squared (kg/m^2). Percentage body fat was calculated on the basis of the Durnin and Womersley (12) equations from the sum of skinfold measurements at the biceps, triceps,

subscapular site, and suprailiac site using Lange calipers. The lean body mass (kg) was subsequently calculated as body weight less fat mass. Muscle mass was calculated from lean body mass using the muscle–to–lean body mass ratio reported by Wang et al. (13). All subjects underwent triple-oxygen scans ($H_2^{15}O$, $C^{15}O$, and $^{15}O_2$) at rest and after exposure to mild cold (15.5°C [60°F]) (Fig. 1). To induce cold stress, the subjects rested in the PET scanner room in minimal clothing 30 min before the ^{15}O stress scans and during the entire ^{18}F-FDG uptake period. The room was held at a temperature of 15.5°C and 2 fans were used to provide low-level airflow, exposing the subjects to a cold airstream. The subjects were closely monitored during the cold-exposure period for signs of shivering and were asked every 5 min to rate their sensation of cold. All subjects reported being very cold after about 20 min, and in some subjects the airflow had to be lowered to prevent shivering. The study was approved by the Institutional Review Board of Wayne State University, and informed consent was obtained from all subjects.

PET Data Acquisition

All subjects were scanned on an EXACT HR PET scanner (Siemens) in 2-dimensional mode to decrease the contribution of scatter from outside the field of view. Initially, 2 venous catheters were established for tracer injection and venous blood sampling. During the entire baseline protocol, the patients were wrapped in warm blankets and rested comfortably inside the PET gantry. The subjects were positioned with the neck–shoulder region in the field of view of the PET scanner, and a 15-min transmission scan was obtained to correct for photon attenuation. Subsequently, the subjects inhaled ^{15}O-labeled oxygen (2,960 MBq [80 mCi]) through a disposable plastic facemask for 5 s (1–2 deep breaths), which coincided with the start of a 2-min dynamic emission scan (60×2 s). Two venous blood samples (0.4 mL) were obtained at the end of the dynamic scan for determination of blood hematocrit level. In addition, arterial oxygen saturation was monitored during the whole dynamic scan using a Dinamap ProCare 400 monitor (GE Healthcare). After a 12-min period to allow for tracer decay, the subjects then inhaled ^{15}O-labeled CO gas (1,850 MBq [50 mCi]) in 1–2 short breaths, and after a 2-min equilibration phase, a 3-min static PET scan was initiated. Six venous blood samples (0.4 mL) were taken during the static scan to measure whole-blood radioactivity during the scanning period. Finally, ^{15}O-water (1,850 MBq [50 mCi]) was injected as a slow bolus over 45 s, and a 2-min dynamic PET scan was obtained (60×2 s). Again, 2 venous blood samples (0.4 mL) were obtained at the end of the dynamic scan and arterial oxygen saturation was monitored during the dynamic sequence as before. These 3 scans were then repeated during mild cold stress, which was induced by removing all blankets from the subjects and letting them rest in the PET scanner in minimal clothing exposed to a temperature of 15.5°C. After a 30-min transition period to reach stable systemic oxygen consumption, the three ^{15}O PET scans were repeated. At the conclusion of the oxygen PET scans (~60 min after the beginning of cold exposure), another 10-min indirect calorimetric measurement was performed to determine cold-stress oxygen consumption. The ^{18}F-FDG tracer (185 MBq [5 mCi]) was then injected, and the subjects remained exposed to a 15.5°C temperature during a 50-min uptake period. At the conclusion of the uptake period, a 10-min static ^{18}F-FDG scan was acquired at the same position as the oxygen scans. Finally, the patient was transported to the nearby PET/CT suite and a whole-body PET/CT scan was obtained to verify the presence of BAT in adipose tissue.

Measurement of Oxygen Saturation Using NIRS

To evaluate whether regional blood oxygen saturation (rSO_2) in BAT, white adipose tissue (WAT), and muscle can be measured noninvasively, we used the INVOS 5100C somatic oxymeter (Somanetics Inc.). The ability of light in the near-infrared spectrum to penetrate several centimeters of tissue allows for the noninvasive measure of oxygenated hemoglobin, primarily in the venous bed. As a result, reduction in rSO_2 reflects increased tissue oxygen

use over supply. Before PET imaging, disposable, noninvasive sensors were attached to the subjects at the location of supraclavicular BAT, shoulder muscle, and abdominal WAT. Data were continuously measured and included time marks to relate rSO_2 values to rest and cold-stress periods. The rSO_2 ratio between BAT and muscle ($R1 = rSO_{2BAT}/rSO_{2muscle}$) and the rSO_2 ratio between BAT and abdominal WAT ($R2 = rSO_{2BAT}/rSO_{2WAT}$) were used to quantitatively assess cold-stimulated oxygen depletion in BAT and WAT.

Whole-Body Indirect Calorimetry

Measurement of energy expenditure (kcal/d) under resting conditions and in response to the cold challenge was performed using the VO2000 Portable Metabolic Testing System (Med-Graphics). The instrument was calibrated against a known gas mixture before each experimental day and autocalibrated between experimental runs. For both the resting and the cold-challenge protocols, subjects were measured while lying in a relaxed position after having fasted for at least 6 h. The room temperature was 25°C (77°F) for the resting measurements and 15.5°C for the cold stress. Subjects were fitted with neoprene face masks, and all measurements were taken using the low-flow pneumotachs. Heart rate (beats/min), volume of oxygen consumption (VO_2; L/min), volume of carbon dioxide production (VCO_2; L/min), and respiratory quotient (RQ; VCO_2/VO_2) were all measured for 15 min under the resting and cold-stress conditions. Whole-body energy expenditure (kcal/d) was then calculated from VO_2 and RQ values, based on the Weir (14) equation using BreezeSuite software (version 6.0; MedGraphics).

Image Data Processing and Analysis

All images were corrected for decay, attenuation, randoms, and scatter. The ^{15}O images were reconstructed using filtered back-projection with a Hanning filter at the Nyquist frequency and were subsequently smoothed with a gaussian filter, resulting in a trans-axial spatial resolution of approximately 10 mm in full width at half maximum. To calculate blood flow and oxygen extraction, the arterial input function needs to be known. It has been shown (15) that the arterial input function can be obtained accurately from the dynamic data themselves, eliminating the need for online blood sampling. This can be achieved by defining regions of interest (ROIs) at the location of the ascending aorta in a blood-pool image obtained using ^{15}O-labeled CO and transferring these ROIs to the dynamic ^{15}O water and $^{15}O_2$ data (16). Using the AMIDE software, a 3-dimensional ROI (1-cm diameter) was defined over the ascending aorta, and spillover from the left atrium was avoided by considering only planes in which the left atrium was not visible. The resulting time–activity curve was subsequently corrected for partial-volume effects by taking into account the diameter of the ascending aorta obtained from CT (2.3 ± 0.3 cm) and the full width at half maximum of the reconstructed PET images (17). Static ^{18}F-FDG data were reconstructed using a Shepp–Logan filter (cutoff frequency, 0.3 cycles per pixel), yielding a transaxial spatial resolution of approximately 6 mm in full width at half maximum. ROIs were defined in ^{18}F-FDG images at the location of brown adipose tissue (BAT), WAT, and muscle and subsequently transferred to the dynamic ^{15}O scans. BAT was considered present if there were areas of tissue that were more than 5 mm in diameter, had the CT density of adipose tissue (–250 to –50 Hounsfield units [HU]), and had a maximal standardized uptake value (SUV) of ^{18}F-FDG of at least 2.0. This cutoff represented more than 2 SDs above the maximal SUV seen in typical depots of WAT. BAT volume was determined by applying a threshold both to the CT image volume ($–250 < HU < –50$) and to the ^{18}F-FDG volume ($SUV > 2.0$) and then applying the logical AND operation to the 2 masks, followed by removal of all areas that were smaller than 0.125 cm^3. The final BAT ROI was chosen at the location of the largest contiguous group of voxels that survived the masking operation. These regions most frequently represented the cervical, supraclavicular, and superior mediastinal depots, superficial and lateral to the sternocleidomastoid muscles (Fig. 2). The

volume of BAT ROIs (cm^3) was converted into weight (g) by assuming a density of 0.90 g/cm^3. Finally, WAT ROIs were defined manually on 2–3 adjacent planes at the location of subcutaneous neck fat, and muscle ROIs were defined at the location of the shoulder–deltoid area.

Dynamic quantitative PET imaging has been established as the gold standard for the in vivo determination of metabolic rate of oxygen (MRO_2) in the brain (18,19) and skeletal muscle (20,21). The accuracy of this method for the measurement of oxygen extraction fraction (OEF) in brain tissue has been validated under physiologic and pathologic conditions over a range of OEF values from 0.05 to 0.80 (19,22). The MRO_2 (mL/100 g/min) in the tissues of interest is calculated as the product of blood flow (mL/100 g/min), OEF (unitless), and arterial oxygen concentration (cO_2; mL O_2/100 mL), which is derived from the patient's arterial oxygen saturation (pSat) and hematocrit (HCT) according to the equation

$$cO_2 \quad (mL \quad O_2/100 \quad mL) = (HCT/3) \times 1.36 \quad pSat + 0.0031 \quad pO_2 \quad (torr),$$

where partial pressure of oxygen (pO_2) was calculated from the measured arterial oxygen saturation according to Severinghaus' (23) formula. Finally, the daily energy expenditure (DEE; kcal/d) was calculated from the obtained MRO_2 and the weight of BAT according to the formula

$$\begin{aligned} DEE \quad (kcal/d) = &MRO_2 \quad (mL/100 \quad g/min) \\ &\times weight \quad of \quad BAT \quad (100 \quad g) \\ &\times 0.0048 \quad (kcal/mL) \\ &\times 1,440 \quad (min/d), \end{aligned}$$

where the conversion factor between kilocalories and milliliters of O_2 was assumed for an RQ of 0.80 (24).

Statistical Analysis

Data are reported as mean ± SD. ^{18}F-FDG uptake in BAT after exposure to mild cold was highly variable, with a few subjects (all women) showing extensive uptake in the cervical–supraclavicular depots whereas most subjects displayed either no BAT or only small pockets of activated BAT (Fig. 2). To account for this skewed distribution, the subjects were divided into 2 groups (high BAT and low BAT), with the threshold being set to 10 g of activated BAT. This threshold was previously reported as the median mass of activated BAT in a large population (5), and we used this value as a meaningful cutoff between patients with high BAT uptake and low BAT uptake. Initially, the Shapiro–Wilk test was applied to assess the normality of variable distributions. Subsequently, normally distributed continuous variables were compared between the 2 groups using an independent-sample *t* test, and nonnormally distributed continuous variables were compared between the 2 groups using the Mann–Whitney *U* test. Finally, correlation between variables was assessed using Pearson *r*. All reported *P* values are 2-tailed, and values of less than 0.05 were considered to indicate statistical significance.

RESULTS

Table 1 shows descriptive statistics for the high-BAT and low-BAT groups. Moreover, because extensive BAT uptake was primarily observed in women, we also present a comparison of values for women only (i.e., comparison-controlled for sex). The average

mass of activated BAT was 59.1 ± 17.5 g (range, 32–85 g) in the high-BAT group (mean age, 29.6 ± 5.5 y) and 2.2 ± 3.6 g (range, 0–9.3 g) in the low-BAT group (mean age, 31.4 ± 9.7 y; Fig. 3A). The high-BAT group consisted almost exclusively of women (8 women and 1 man), whereas the low-BAT group was about equally divided between the sexes (9 men and 7 women), a result suggesting that women have a greater capacity to increase BAT activity. In accordance with the experimental design, corresponding maximal SUV was found to be significantly higher in the high-BAT group than in the low-BAT group (10.7 ± 3.9 vs. 2.1 ± 0.7, $P = 0.01$; Fig. 3B). Because of the sex differences in the presence of BAT, the male-dominated low-BAT group showed a trend toward higher levels of lean body mass (54 + 11 vs. 46 + 7 kg, $P = 0.09$; Fig. 3C). Conversely, the 2 groups did not differ in body mass index (22.1 + 3.1 vs. 24.7 + 3.9 kg/m^2, $P = 0.39$). Plots showing the relationship between BAT mass and lean body mass and between BAT mass and body mass index are presented in the supplemental material, which is available online at http://jnm.snmjournals.org.

As expected from previous work (25,26), the 2 groups (high-BAT and low-BAT) showed different responses to exposure to mild cold. Whereas in the high-BAT group the DEE increased by 17.4% ± 15.0% (from 1,452 to 1,689 kcal/d, $P = 0.02$), DEE remained, on average, virtually constant in the low-BAT group, at 0.4% ± 16%, (change, 1,676–1,643 kcal/d) (Table 1). Moreover, whereas absolute changes in DEE were always positive in the high-BAT group (range, 83–424 kcal/d; mean, 236 ± 205 kcal/d), DEE changes in the low-BAT group varied considerably (range, –397 to 394 kcal/d; mean, –39 ± 287 kcal/d). Finally, the RQ was marginally lower in the high-BAT group (0.83 ± 0.06 in the high-BAT group and 0.91 ± 0.10 in the low-BAT group, $P = 0.15$), suggesting greater levels of resting fat oxidation in this group (27). RQ values were not significantly affected by cold stress (Table 1).

Blood Flow and MRO$_2$ in BAT, WAT, and Muscle

Absolute blood flow values were significantly higher in the high-BAT group than in the low-BAT group only in BAT regions. In the high-BAT group, resting BAT blood flow was 10.8 ± 4.6 mL/100 g/min and increased to 15.9 ± 5.0 mL/100 g/min ($P < 0.01$). Moreover, although in the low-BAT group the blood flow values were lower at both rest and cold stress (5.8 ± 1.7 vs. 6.7 + 2.6 mL/100 g/min, Fig. 4A), the increase was also significant ($P = 0.01$). In WAT, blood flow values were higher overall in the high-BAT group than in the low-BAT group (7.2 ± 3.4 vs. 5.7 ± 2.3 mL/100 g/min, $P = 0.03$; Fig. 4B), although no significant increases were determined between rest and cold stress in either group. Finally, blood flow values were similar for both groups in muscle regions (4.4 ± 1.9 vs. 3.9 ± 1.7 mL/100 g/min, $P = 0.32$). Plots showing the relationship between BAT mass and blood flow, muscle, and WAT are included in the supplemental material.

The OEF was found to be similar in both groups in BAT, muscle, and WAT regions. Specifically, overall OEF in BAT was determined as 0.51 ± 0.17 in the high-BAT group and 0.47 ± 0.18 in the low-BAT group ($P = 0.41$). Similarly, OEF values in muscle were 0.31 ± 0.06 and 0.32 ± 0.08 in the high-BAT and low-BAT groups, respectively ($P = 0.68$), and were slightly higher in WAT regions (0.41 ± 0.13 vs. 0.38 ± 0.12, $P = 0.31$).

Calculated MRO$_2$ values in BAT based on corresponding blood flow and OEF values were highest in the high-BAT group during both rest and cold exposure (Fig. 5A). MRO$_2$ estimates increased from a mean resting value of 0.97 ± 0.53 mL/100 g/min to a mean value of 1.42 ± 0.68 mL/100 g/min ($P = 0.04$) during cold exposure. These MRO$_2$ values in BAT were significantly higher than those determined in the low-BAT group (0.40 ± 0.28 at rest and 0.51 ± 0.23 during cold exposure, $P = 0.67$). In comparison, MRO$_2$ estimates in muscle tissue were similar during rest and cold exposure in both groups (~0.20 ± 0.11 mL/100 g/

min). In contrast, MRO_2 values in WAT were significantly higher in the high-BAT group than in the low-BAT group both at rest (0.48 ± 0.07 vs. 0.26 ± 0.16 mL/100 g/min, $P = 0.03$) and during cold stress (0.54 ± 0.09 vs. 0.30 ± 0.23 mL/100 g/min, $P = 0.04$) (Fig. 5A). Finally, we determined a significant correlation between blood flow and the MRO_2 ($r^2 = 0.90$, $P = 0.01$; Fig. 5B), suggesting that oxidative metabolism is the main determinant of BAT perfusion.

Energy Consumption of BAT and Muscle

The DEE associated with BAT oxidative metabolism was highly variable in the high-BAT group, with an average of 3.2 ± 2.4 kcal/d (range, 1.9–4.6 kcal/d) at rest and 6.3 ± 3.5 kcal/d (range, 4.0–9.9 kcal/d) during cold stress. These values were significantly higher than those in the low-BAT group, which were determined as $0.14 + 0.12$ kcal/d (range, 0–0.38 kcal/d). A high correlation between blood flow values and DEE in activated BAT was determined ($r^2 = 0.66$; Fig. 6A), indicating that blood flow is the main predictor of BAT energy expenditure. Moreover, to assess the upper limit for DEE in activated BAT, we also present DEE values for BAT mass derived using a less stringent cutoff threshold (SUV = 1.5) and assuming almost complete extraction of oxygen from blood (OEF, 0.95). Finally, we also observed a significant relationship between maximal SUVs in BAT and the corresponding DEE in BAT ($r^2 = 0.65$, $P = 0.02$; Fig. 6B).

No statistically reliable effect of cold was observed on deltoid muscle oxidative metabolism in either high-BAT or low-BAT subjects. Indeed, the cold-induced increase in energy expenditure observed in high-BAT subjects was modestly inversely related to muscle oxidative metabolism.

Relationship Between NIRS Measures and MRO_2

To determine whether noninvasive NIRS can be used to assess oxygen consumption, we examined the correlations of the R1 and R2 ratios with MRO_2 values derived from PET imaging. R1 values tended to be lower in subjects with active BAT ($P = 0.08$, Fig. 7A); however, no differences in R2 were found between groups with and without BAT. In the high-BAT group, a significant inverse correlation between MRO_2 and R1 ($P = 0.02$, $r^2 = 0.46$) was determined in BAT during resting and cold conditions, indicating increased oxygen depletion in venous blood at high MRO_2 values (Fig. 7B). In contrast, no significant correlation between R1 and MRO_2 was observed in the low-BAT group, nor was there any correlation between MRO_2 and the R2 ratio in either group.

DISCUSSION

Recent work has clearly established the presence of symmetric adipose depots in the cervical and supraclavicular region of humans which, in a subset of individuals, can be induced to greatly increase ^{18}F-FDG tracer uptake in response to cold stress. These depots contain UCP1-positive multilocular adipocytes, and the fat cells within these depots express genes that are known to be enriched in brown adipocytes (6). It has been estimated that 50 g of human BAT having the thermogenic activity of cold-adapted rodent BAT might expend as much as 20% of daily energy intake (28) and thus might be a rational target for antiobesity therapeutics. Despite these intriguing and potentially promising results, so far oxidative metabolism in human BAT has been assessed only indirectly using ^{11}C-acetate PET, a surrogate marker of tissue VO_2 (29). Hence, our objective was to directly evaluate oxidative metabolism in human BAT and its relation to ^{18}F-FDG tracer uptake and total energy expenditure.

Our results confirm recent experiments examining cold-induced ^{18}F-FDG uptake in human BAT. The current study demonstrated that mild cold exposure led to high ^{18}F-FDG tracer uptake in BAT in about a third of the subjects, whereas about half the subjects showed no ^{18}F-FDG tracer uptake, with the rest displaying low-level ^{18}F-FDG tracer uptake in scattered supraclavicular BAT depots. In high-BAT subjects, we observed cervical–subclavicular depots with a median mass of about 60 g and a cold-induced ^{18}F-FDG maximal SUV of about 9, values that are in close agreement with numerous published reports (6). Moreover, similar to previous reports (5), we found a higher mass and activity of BAT in women than in men, with a ratio of approximately 3:1. Our study group consisted entirely of young adults; thus, no relationship between BAT activation and age or body mass index was observed.

The baseline blood flow in BAT of subjects with high ^{18}F-FDG tracer uptake was about twice that of subjects with low ^{18}F-FDG uptake (10 vs. 5 mL/100 g/min) and increased by about 50% during cold stress (to ~15 mL/100 g/min). Moreover, semiquantitative assessment of glucose metabolism in BAT based on ^{18}F-FDG maximal SUV showed a significant correlation with the calculated MRO_2, suggesting that at least part of the glucose transported into adipose tissue undergoes oxidative metabolism.

Direct measurement of oxidative metabolism in cervical–subclavicular BAT depots demonstrated that mild cold stress increased the median oxygen consumption of these BAT depots to about 12 kcal/d/100 g, or about 7 kcal/d for a typical subject with 60 g of BAT. Because tissue MRO_2 (consumption) is the product of blood flow and OEF, blood flow sets the upper limit on tissue oxygen consumption. In this regard, we note that the cold-induced increase in cervical–subclavicular BAT blood flow was nearly identical to that recently reported by Orava et al. (25). Thus, blood flow data from both laboratories indicate that acutely activated human BAT contributes very little to cold-induced energy expenditure, even if one assumes close to 100% OEF. Based on the measured blood flow values and assuming almost complete blood oxygen extraction and a generous estimation of BAT mass, the daily energy consumption in BAT appears to be in the range of 15–25 kcal/d (Fig. 6A). These values are consistent with recent tracer experiments showing that the energy content of glucose (25) or nonesterified fatty acids (29) taken up by active BAT is trivial when compared with cold-induced energy expenditure (30). Although it has been suggested, in analogy to rat data (8), that cold-induced BAT thermogenesis in humans relies on oxidation of fatty acids mobilized from brown adipocytes (31), there are only indirect data implying this phenomenon (29).

Speculation regarding the functional importance of human BAT has often invoked comparisons with rodent models of BAT function. In this regard, the classic experiments by Foster and Frydman (32) demonstrated that exposure to cold increases BAT blood flow by a factor of 10- to 20-fold, achieving a maximal rate of more than 1,000 mL/100 g/min. This rate is 100 times greater than that observed in humans. Similarly, maximal glucose up-take rates in rodent BAT are at least 10-fold greater than those observed in human BAT. In the case of human BAT, various investigators (6,25) reported that the energy content of cold-induced glucose uptake amounted to less than 10 kcal/d if fully oxidized, in agreement with our findings.

The relatively low metabolic rate of human BAT depots is not entirely unexpected. Available histologic data on adult humans indicate that cervical–supraclavicular BAT depots contain a mixture of multilocular brown adipocytes interspersed within a greater volume of unilocular white adipocytes (33), which have much lower metabolic activity. The presence of a brown–white adipocyte mixture in the neck region can also be inferred from the increased MRO_2 at the presumed location of BAT (as compared with WAT) in the low-BAT

group. Because PET imaging lacks the resolution to measure microscopic patches of brown adipocytes, data derived from PET analysis necessarily reflect the average metabolism of a mixed-cell population. Thus, although various amounts of active brown adipocytes clearly exist within these depots, the average oxidative activity of the depots may be relatively low.

It is now well established that cold stress increases the oxidative metabolism in human BAT depots (29). Recent studies have shown that systemic nonselective β-adrenergic stimulation by drugs such as ephedrine (26) or isoproterenol (34), at concentrations that increase energy expenditure to the same extent as cold exposure, does not activate BAT in humans. We and others (30) have observed that cold-induced increases in whole-body energy expenditure (average of ~250 kcal/d in the present study) strongly correlate with the presence of cold-activated BAT depots. Nonetheless, these PET-defined BAT depots account for less than 5% of the total cold-induced increase in metabolism. Thus, most cold-induced thermogenesis does not involve PET-defined BAT depots, although a common physiologic network likely mediates both. How to reconcile these finding is presently unclear. The lower RQ of high-BAT subjects suggests that this process involves mobilization and oxidation of fat. The existence of cold-induced thermogenesis that is independent of BAT is well documented, particularly in warmth-adapted animals (32). It seems likely that cold-induced increases in metabolism might involve relatively small changes in large organ systems that would be difficult to detect by standard PET imaging techniques. Skeletal muscle contributes substantially to the whole-body metabolic rate and has been implicated in adaptive thermogenesis in humans (7,35). We have assessed the increases in total skeletal muscle energy expenditure during mild cold stress based on the measured energy expenditure in the deltoid muscle. At present we have no clear evidence that muscle contributes to thermogenesis induced by mild cold stress; however, it is difficult to draw conclusions on the potential contribution of muscle in our experiments, which evaluated a single muscle group. Moreover, even when the energy expenditure derived from neck fat is considered representative of abdominal fat, the increase in WAT energy expenditure accounts for only about 30% of total body expenditure. All in all, it appears that BAT, muscle, and WAT together account for only about half the increase in total-body energy expenditure during cold stress, even if one assumes significant brown adipocytes interspersed in abdominal fat. The source of the other 50% increase is currently unknown and warrants further, more detailed studies. It is conceivable, however, that cold-induced thermogenesis in humans involves activation of brown adipocytes in WAT depots that are too diffuse to be imaged by PET. Rodent WAT contains variable amounts of "brown-like" or "beige" adipocytes that can be recruited by cold stress and adrenergic agonists (36). It has recently been proposed that most, if not all, BAT in adult humans (including supraclavicular) is this type (37). In rodents, these brown adipocytes are derived from a unique cell lineage, and their appearance is a highly variable genetic trait (38). If the same is true for humans, then widely distributed brown–beige adipocytes might help explain why an elevated metabolic rate was observed only in high-BAT subjects.

Our data indicate that the metabolic rate of WAT is about twice that of muscle—a finding that runs counter to the literature. Whereas the resting oxygen consumption in muscle of about 0.2 mL/100 g/min (equivalent to 12 kcal/kg/d) is in the expected range (13), the observed WAT oxygen consumption of 0.3–0.5 mL/100 g/min (equivalent to 18–30 kcal/kg/d) appears to be very high, especially in the high-BAT group. The most likely reason for this discrepancy is that neck WAT regions have a mixture of brown and white adipocytes that differ significantly in composition from abdominal WAT. This hypothesis is substantiated by our observation of lower HU (denser tissue) in neck WAT regions (~20%) than in abdominal WAT, in addition to somewhat higher SUVs in neck WAT regions. Because of the limited axial field of view for dynamic PET imaging, WAT regions had to be defined in areas that most likely do not represent depots of pure white adipocytes. In this regard it is

interesting that the observed MRO_2 in WAT of the neck region in the high-BAT group was about twice that observed in the low-BAT group, indicating varying mixtures of brown and white adipocytes in neck fat tissue. On the other hand, the MRO_2 of WAT in both groups was almost unchanged by cold stress. Additional quantitative studies, especially in abdominal WAT, will be required to identify alternative sites and mechanisms of cold-induced thermogenesis in humans.

Although dynamic PET imaging allows accurate quantification of oxidative metabolism in BAT, routine monitoring of BAT activity is likely to be facilitated by more noninvasive technologies that do not rely on intravenous administration of radioactive compounds. Of these, NIRS allows an indirect, noninvasive, and dynamic measure of supraclavicular BAT oxygen consumption, even though the spatial accuracy is limited to about 15 mm at a depth of 30 mm. Thus, especially for heterogeneous tissue such as BAT, the signal might be contaminated by contributions from other tissues. The rationale for the use of NIRS is based on the classic experiments by Foster and Frydman (32), who demonstrated that oxygen consumption in activated BAT is limited by oxygen delivery. Thus, BAT activation produces a sustained decrease in venous oxygen concentration, which can be detected by NIRS (Fig. 7A). Our studies showed a significant correlation between PET-derived MRO_2 and NIRS in subjects with activated BAT, suggesting that NIRS can be used in these subjects as an indirect measure of oxidative metabolism.

There are limitations associated with our study. The definition of BAT mass based on maximal ^{18}F-FDG SUV is problematic because supraclavicular adipose tissue is a mixture of brown and white adipocytes with unknown proportions. Clinically, a maximal SUV of greater than 3 was used by Baba et al. (39) to define high ^{18}F-FDG uptake in BAT, whereas a maximal SUV of less than 2 was used to define low ^{18}F-FDG uptake in BAT. Moreover, those investigators also reported a significant correlation between CT HU and maximal SUV, indicating that tissue associated with a maximal SUV of less than 2 has a median HU value of about –100, most likely representing typical WAT (-92 ± 25 HU). More important, Orava et al. (25) quantified glucose metabolic rate in adipose tissue and used a rate of 3.0 umol/100 g/min during cold exposure to represent active BAT. Those authors justified this threshold by assessing the BAT glucose uptake rate under control conditions, which were always lower than 1.7 μmol/100 g/min. Using this cutoff threshold, those investigators reported the estimated mass of detected active BAT to be in the range of 9–90 g (mean, 34 ± 22), a value that compares favorably with our estimates of BAT mass after cold exposure (range, 0–85 g; mean, 32 ± 31). In recognition of the problem of defining BAT on the basis of significant ^{18}F-FDG uptake, we reanalyzed our data using an SUV threshold of 1.5 to assess the amount of BAT mass according to this less conservative threshold. This analysis showed an excellent correlation ($r^2 = 0.94$) between BAT mass derived using an SUV threshold of 2.0 and BAT mass derived using an SUV threshold of 1.5, with a proportionality factor of 0.65. Another limitation might be the potential underestimation of OEF due to the fact that the triple-oxygen method was initially developed for the brain and was not optimized for other tissues, although it was used successfully in muscle (40). Because our OEF values in muscle closely corresponded to the published values, we believe that the OEF values we obtained for BAT and WAT are correct. However, we cannot completely exclude a slight underestimation of the OEF values for BAT. To address this limitation, we have calculated BAT energy consumption for almost complete blood oxygen extraction (OEF = 0.95), which certainly represents the upper limit for BAT energy expenditure. Because of the long study protocol, the triple-oxygen protocol started 30 min after the start of cold exposure, with the $^{15}O_2$ and $C^{15}O$ inhalation being performed first. Blood flow measurements using ^{15}O-labeled water were performed about 60 min after the start of cold exposure, followed immediately by ^{18}F-FDG tracer injection. Thus, the standard protocol (i.e., 60 min of cold exposure) applied at least to blood flow and ^{18}F-FDG

uptake assessment. Accordingly, our blood flow values in BAT, WAT, and muscle are almost identical to those reported by Orava et al. (25) using a very different cold-stress protocol (2 h of exposure at 17°C).

CONCLUSION

The main result of our study is that BAT thermogenesis in humans accounts for 15–25 kcal/d during mild cold stress, even in subjects with relatively large BAT depots. Furthermore, it appears that because of the large difference in both blood flow and glucose metabolic rate in BAT between humans and rodents, the application of rodent data to humans is problematic and needs careful assessment.

Supplementary Material

Refer to Web version on PubMed Central for supplementary material.

Acknowledgments

REFERENCES

1. Foster DO, Frydman ML. Tissue distribution of cold-induced thermogenesis in conscious warm- or cold-acclimated rats reevaluated from changes in tissue blood flow: the dominant role of brown adipose tissue in the replacement of shivering by nonshivering thermogenesis. Can J Physiol Pharmacol. 1979; 57:257–270. [PubMed: 445227]

2. Nedergaard J, Golozoubova V, Matthias A, Asadi A, Jacobsson A, Cannon B. UCP1: the only protein able to mediate adaptive non-shivering thermogenesis and metabolic inefficiency. Biochim Biophys Acta. 2001; 1504:82–106. [PubMed: 11239487]

3. Dawkins MJ, Scopes JW. Non-shivering thermogenesis and brown adipose tissue in the human new-born infant. Nature. 1965; 206:201–202. [PubMed: 5830159]

4. Blaza S. Brown adipose tissue in man: a review. J R Soc Med. 1983; 76:213–216. [PubMed: 6834374]

5. Cypess AM, Lehman S, Williams G, et al. Identification and importance of brown adipose tissue in adult humans. N Engl J Med. 2009; 360:1509–1517. [PubMed: 19357406]

6. Virtanen KA, Lidell ME, Orava J, et al. Functional brown adipose tissue in healthy adults. N Engl J Med. 2009; 360:1518–1525. [PubMed: 19357407]

7. van Marken Lichtenbelt WD, Vanhommerig JW, Smulders NM, et al. Cold-activated brown adipose tissue in healthy men. N Engl J Med. 2009; 360:1500–1508. [PubMed: 19357405]

8. Ma SW, Foster DO. Uptake of glucose and release of fatty acids and glycerol by rat brown adipose tissue in vivo. Can J Physiol Pharmacol. 1986; 64:609–614. [PubMed: 3730946]

9. Nedergaard J, Bengtsson T, Cannon B. Unexpected evidence for active brown adipose tissue in adult humans. Am J Physiol Endocrinol Metab. 2007; 293:E444–E452. [PubMed: 17473055]

10. Muzik O, Mangner TJ, Granneman JG. Assessment of oxidative metabolism in brown fat using PET imaging. Front Endocrinol. 2012; 3:1–7.

11. Lohman, TG.; Roche, AF.; Martorel, R. Anthropometric Standardization Reference Manual. Human Kinetics Books; Champaign, IL: 1988. p. 53

12. Durnin JVA, Womersley J. Body fat assessed from the total body density and its estimation from skinfold thickness: measurements on 481 men and women aged from 16 to 72 years. Br J Nutr. 1974; 32:77–97. [PubMed: 4843734]

13. Wang Z, Ying Z, Bosy-Westphal A, et al. Evaluation of specific metabolic rates of major organs and tissues: comparison between men and women. Am J Hum Biol. 2011; 23:333–338. [PubMed: 21484913]

14. Weir JB. New methods for calculating metabolic rate with special reference to protein metabolism. J Physiol Lond. 1949; 109:1–9. [PubMed: 15394301]

15. Hermansen F, Rosen SD, Fath-Ordoubadi F, et al. Measurement of myocardial blood flow with oxygen-15 labelled water: comparison of different administration protocols. Eur J Nucl Med. 1998; 25:751–759. [PubMed: 9662598]

16. van der Veldt AA, Hendrikse NH, Harms HJ, et al. Quantitative parametric perfusion images using 15O-labeled water and a clinical PET/CT scanner: test–retest variability in lung cancer. J Nucl Med. 2010; 51:1684–1690. [PubMed: 20956480]

17. Germano G, Chen BC, Huang SC, Gambhir SS, Hoffman EJ, Phelps ME. Use of the abdominal aorta for arterial input function determination in hepatic and renal PET studies. J Nucl Med. 1992; 33:613–620. [PubMed: 1552350]

18. Frackowiak RS, Lenzi GL, Jones T, Heather JD. Quantitative measurement of regional cerebral blood flow and oxygen metabolism in man using 15O and positron emission tomography: theory, procedure, and normal values. J Comput Assist Tomogr. 1980; 4:727–736. [PubMed: 6971299]

19. Mintun MA, Raichle ME, Martin WR, Herscovitch P. Brain oxygen utilization measured with O-15 radiotracers and positron emission tomography. J Nucl Med. 1984; 25:177–187. [PubMed: 6610032]

20. Ruotsalainen U, Raitakari M, Nuutila P, et al. Quantitative blood flow measurement of skeletal muscle using oxygen-15-water and PET. J Nucl Med. 1997; 38:314–319. [PubMed: 9025761]

21. Kalliokoski KK, Kemppainen J, Larmola K, et al. Muscle blood flow and flow heterogeneity during exercise studied with positron emission tomography in humans. Eur J Appl Physiol. 2000; 83:395–401. [PubMed: 11138581]

22. Hattori N, Bergsneider M, Wu HM, et al. Accuracy of a method using short inhalation of ^{15}O-O_2 for measuring cerebral oxygen extraction fraction with PET in healthy humans. J Nucl Med. 2004; 45:765–770. [PubMed: 15136624]

23. Severinghaus JW. Pulmonary vascular function. Am Rev Respir Dis. 1977; 115:149–158. [PubMed: 869311]

24. Leonard WR. Measuring human energy expenditure and metabolic function: basic principles and methods. J Anthropol Sci. 2010; 88:221–230. [PubMed: 20834061]

25. Orava J, Nuutila P, Lidell ME, et al. Different metabolic responses of human brown adipose tissue to activation by cold and insulin. Cell Metab. 2011; 14:272–279. [PubMed: 21803297]

26. Cypess AM, Chen YC, Sze C, et al. Cold but not sympathomimetics activates human brown adipose tissue in vivo. Proc Natl Acad Sci U S A. 2012; 109:10001–10005. [PubMed: 22665804]

27. McArdle, WD.; Katch, FI.; Katch, VL. Exercise Physiology: Energy, Nutrition, and Human Performance. 5th ed.. Lippincott, Williams and Wilkins; Philadelphia, PA: 2001. p. 132

28. Rothwell NJ, Stock MJ. Luxusconsumption, diet-induced thermogenesis and brown fat: the case in favour. Clin Sci (Lond). 1983; 64:19–23. [PubMed: 6337007]

29. Ouellet V, Labbé SM, Blondin DP, et al. Brown adipose tissue oxidative metabolism contributes to energy expenditure during acute cold exposure in humans. J Clin Invest. 2012; 122:545–552. [PubMed: 22269323]

30. Yoneshiro T, Aita S, Matsushita M, et al. Brown adipose tissue, whole-body energy expenditure, and thermogenesis in healthy adult men. Obesity (Silver Spring). 2011; 19:13–16. [PubMed: 20448535]

31. Ravussin E, Galgani JE. The implication of brown adipose tissue for humans. Annu Rev Nutr. 2011; 31:33–47. [PubMed: 21548774]

32. Foster DO, Frydman ML. Nonshivering thermogenesis in the rat. II. Measurements of blood flow with microspheres point to brown adipose tissue as the dominant site of the calorigenesis induced by noradrenaline. Can J Physiol Pharmacol. 1978; 56:110–122. [PubMed: 638848]

33. Zingaretti MC, Crosta F, Vitali A, et al. The presence of UCP1 demonstrates that metabolically active adipose tissue in the neck of adult humans truly represents brown adipose tissue. FASEB J. 2009; 23:3113–3120. [PubMed: 19417078]

34. Vosselman MJ, van der Lans AA, Brans B, et al. Systemic b-adrenergic stimulation of thermogenesis is not accompanied by brown adipose tissue activity in humans. Diabetes. 2012; 61:3106–3113. [PubMed: 22872233]

35. Wijers SL, Schrauwen P, Saris WH, van Marken Lichtenbelt WD. Human skeletal muscle mitochondrial uncoupling is associated with cold induced adaptive thermogenesis. PLoS ONE. 2008; 3:e1777. [PubMed: 18335051]

36. Cinti S. Between brown and white: novel aspects of adipocyte differentiation. Ann Med. 2011; 43:104–115. [PubMed: 21254898]

37. Wu J, Boström P, Sparks LM, et al. Beige adipocytes are a distinct type of thermogenic fat cell in mouse and human. Cell. 2012; 150:366–376. [PubMed: 22796012]

38. Kozak LP, Koza RA, Anunciado-Koza R. Brown fat thermogenesis and body weight regulation in mice: relevance to humans. Int J Obes. 2010; 34:23–27.

39. Baba S, Jacene HA, Engles JM, Honda H, Wahl RL. CT Hounsfield units of brown adipose tissue increase with activation: preclinical and clinical studies. J Nucl Med. 2010; 51:246–250. [PubMed: 20124047]

40. Kalliokoski KK, Oikonen V, Takala TO, Sipilä H, Knuuti J, Nuutila P. Enhanced oxygen extraction and reduced flow heterogeneity in exercising muscle in endurance-trained men. Am J Physiol Endocrinol Metab. 2001; 280:E1015–E1021. [PubMed: 11350784]
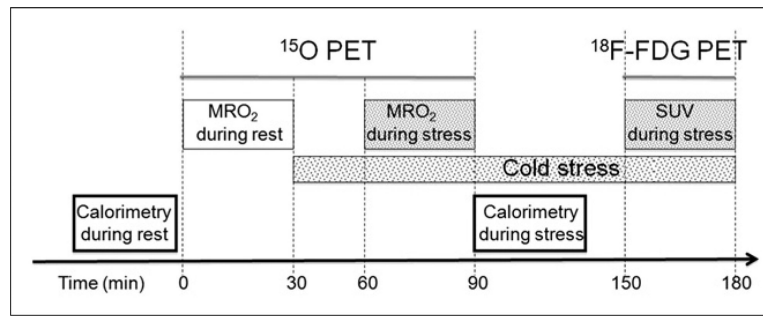
FIGURE 1.
PET protocol used to quantify MRO$_2$ in BAT at rest and during cold stress. After quantitative assessment of oxidative metabolism, patient underwent ^{18}F-FDG PET/CT to correlate MRO$_2$ with ^{18}F-FDG–derived SUV measures. Indirect calorimetry was performed at rest and during exposure to cold stress.
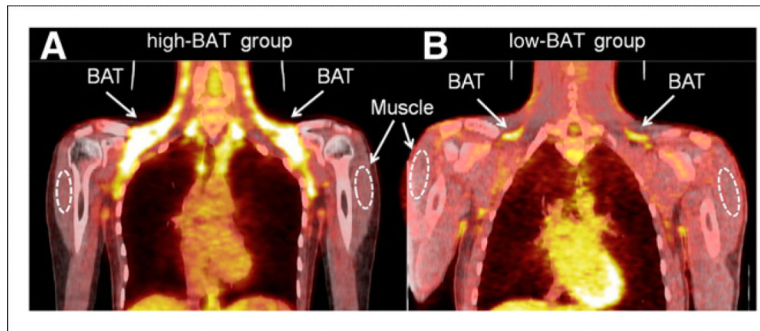
FIGURE 2.
Representative images showing BAT ^{18}F-FDG uptake in subjects belonging to high-BAT and low-BAT groups. Presence of cold-activated BAT was derived on basis of combined conditions of HU range (–250 to –50) and SUV >. 2. ROIs were defined at location of shoulder muscle (broken line) and WAT (not shown). (A) Nine of 25 subjects showed spatially extensive cold-activated BAT (high-BAT group, mass > 10 g). (B). The remaining 16 subjects showed either no cold-activated BAT or only small depots (low-BAT group, mass < 10 g).
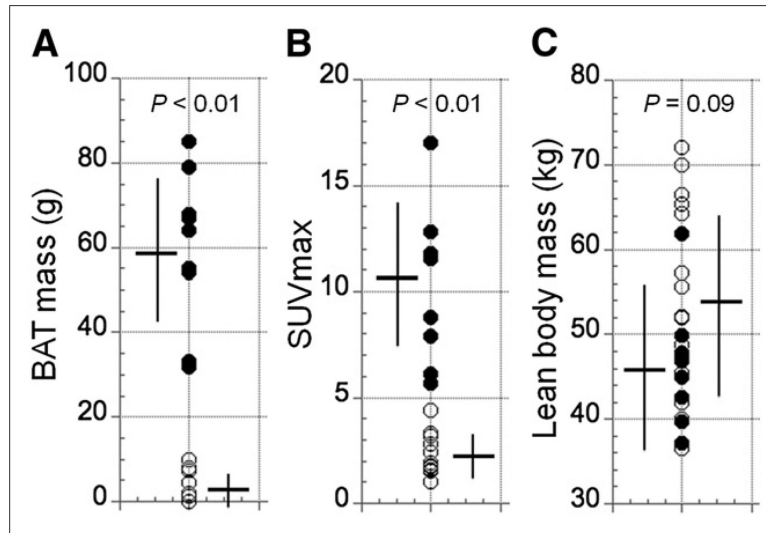
FIGURE 3.
Distribution of amount of BAT mass, maximal SUV, and lean body mass in high-BAT
group (●, *n* = 9, 8 women and 1 man) and in low-BAT group (○, *n* = 16, 7 women and 9
men). Error bars represent SD of measurements. (A) Amount of BAT mass was highly
variable, displaying bimodal distribution. Accordingly, subjects were stratified into high-
BAT and low-BAT groups. (B) Maximal SUV in BAT was significantly higher in high-
BAT group than in low-BAT group ($P < 0.01$). (C) Because of higher male-to-female ratio
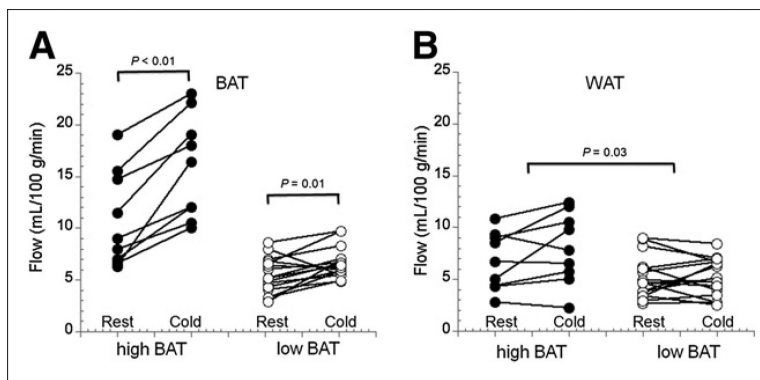in low-BAT group, lean body mass showed tendency toward higher values in low-BAT
group.

FIGURE 4.
Absolute blood flow during rest and cold stress in BAT and WAT in high-BAT and low-BAT groups. (A) Blood flow in activated BAT (high-BAT) is about 50% higher than in nonactivated BAT (low-BAT). Increase in blood flow was significantly higher in high-BAT group than in low-BAT group, although both increases were significant between rest and cold stress. (B) Blood flow in WAT was significantly higher in high-BAT group at both rest and cold stress than in low-BAT group. However, no significant differences were observed between rest and cold stress in either group.
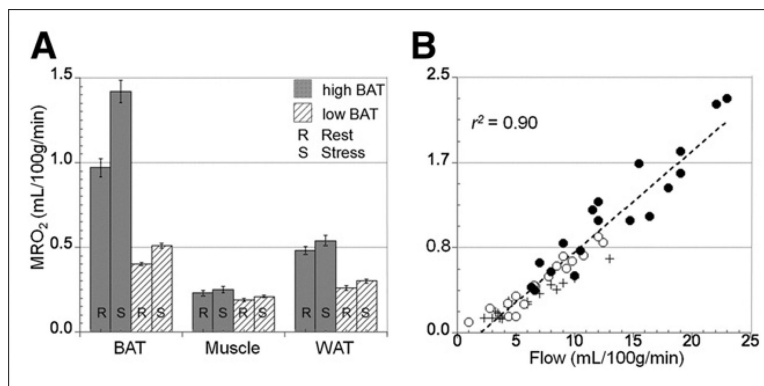
FIGURE 5.
MRO$_2$ in BAT, muscle, and WAT observed in high-BAT and low-BAT groups. Error bars represent SEM. (A) In high-BAT group, MRO$_2$ in BAT at rest was about twice as high as that in low-BAT group. After cold exposure, MRO$_2$ increased by about 50% in high-BAT group but remained at same level in low-BAT group. In contrast, MRO$_2$ in WAT was higher in low-BAT group both at rest and at cold exposure. Finally, MRO$_2$ in muscle was similar for both groups at rest and after cold exposure. (B) Highly significant correlation ($P = 0.01$) was observed between MRO$_2$ in BAT (●), WAT (○), and muscle (×) tissue, indicating that tissue perfusion is main determinant of oxidative metabolism in all 3 types of tissue.
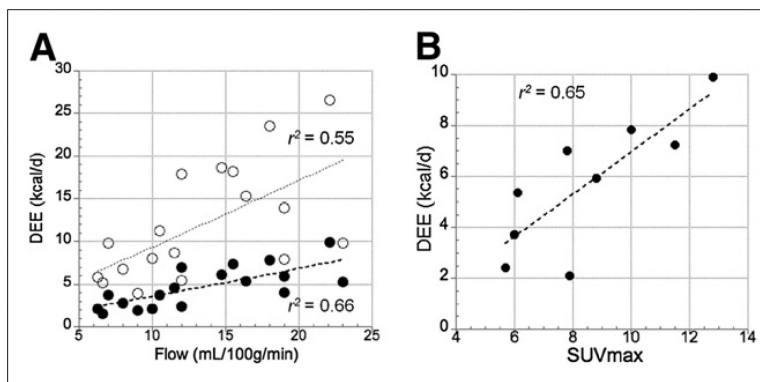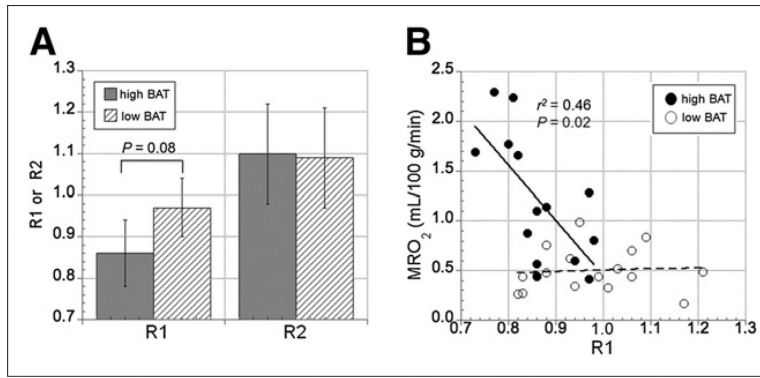
FIGURE 6.
(A) Relationship between blood flow in BAT (both at rest and during stress) and BAT DEE (●), as well as estimates of upper limit for BAT DEE (○), calculated using almost complete oxygen extraction (OEF = 0.95) and generous estimate of activated BAT mass (SUV threshold of 1.5). Maximal contribution of activated BAT to DEE is in range of 15–25 kcal/d. We determined significant correlation ($P = 0.03$), indicating that tissue perfusion is an important determinant of DEE in activated BAT. (B) Correlation between maximal SUV in BAT and DEE in those subjects who had SUV > 2.0 (indicative of activated BAT). We found significant correlation between glucose uptake and DEE ($P = 0.02$).

FIGURE 7.
NIRS-derived measures (R1 and R2) in BAT and WAT. (A) Comparison between R1 and R2 in high-BAT (gray bars) and low-BAT (hatched bars) groups. Consistent with higher BAT oxygen depletion in high-BAT group, R1 ratio in this group tended to be significantly lower than in low-BAT group ($P = 0.08$). R2 ratios were similar in both groups, indicating that oxygen demand in abdominal subcutaneous WAT is comparable in the 2 groups. (B) Relationship between BAT MRO_2 and R1 in both high-BAT (●) and low-BAT (○) groups. Significant correlation between R1 and MRO_2 was observed in high-BAT group, indicating higher oxygen depletion in venous blood (reflected in low R1 values) at high MRO_2 in BAT. In contrast, no significant relationship between R1 and MRO_2 was found in low-BAT group.

TABLE 1

Descriptive Statistics of Subjects in High-BAT and Low-BAT Groups

Parameter	All subjects			Women only		
	High BAT (*n* = 9)	Low BAT (*n* = 16)	*P*	High BAT (*n* = 8)	Low BAT (*n* = 7)	*P*
Age (y)	29.6 ± 5.5	31.4 ± 9.7	NS	28.8 ± 5.2	29.9 ± 7.6	NS
LBM (kg)	46.5 ± 7.1	54.1 ± 11.0	0.04	45.0 ± 3.3	43.9 ± 5.3	NS
BMI (kg/m^2)	22.1 ± 3.1	24.7 ± 3.9	NS	21.3 ± 2.4	22.7 ± 4.5	NS
BSA (m^2)	1.73 ± 0.17	1.89 ± 0.25	NS	1.70 ± 0.14	1.69 ± 0.14	NS
BAT mass (g)	59.1 ± 17.5	2.2 ± 3.6	0.01[*]	56.6 ± 17.0	1.7 ± 4.3	0.01[*]
Maximal SUV	10.7 ± 3.9	2.1 ± 0.9	0.01	10.7 ± 3.9	1.8 ± 0.6	0.01
RQ	0.83 ± 0.06	0.91 ± 0.10	0.08	0.84 ± 0.06	0.88 ± 0.04	NS
ΔRQ (%)	0.2 ± 8.8	−3.53 ± 9.2	NS	−0.9 ± 8.7	−0.03 ± 11.5	NS
DEE (kcal/d)	1,452 ± 242	1,676 ± 480	NS	1,458 ± 258	1,256 ± 209	NS
ΔDEE (%)	17.4 ± 15.0	0.4 ± 15.6	0.04	18.0 ± 16.1	13.6 ± 11.3	NS

NS = not significant at the 0.05 level; LBM = lean body mass; BMI = body mass index; BSA = body surface area; RQ = respiratory quotient.

[*] Nonparametric Mann-Whitney *U* test.